CEIG – Spanish Computer Graphics Conference (2019)
A. Jarabo and D. Casas (Editors)

# Sensitivity Analysis in Shape Optimization using Voxel Density Penalization

D. Montoya-Zapata[1,2], D. A. Acosta[3], A. Moreno[†2], J. Posada[2] and O. Ruiz-Salguero[1]

[1]Laboratory of CAD CAM CAE, Universidad EAFIT, Colombia
[2]Vicomtech, Spain
[3]Grupo de Desarrollo y Diseño de Procesos (DDP), Universidad EAFIT, Colombia

**Abstract**

*Shape optimization in the context of technical design is the process by which mechanical demands (e.g. loads, stresses) govern a sequence of piece instances, which satisfy the demands, while at the same time evolving towards more attractive geometric features (e.g. lighter, cheaper, etc.). The SIMP (Solid Isotropic Material with Penalization) strategy seeks a redistribution of local densities of a part in order to stand stress / strain demands. Neighborhoods (e.g. voxels) whose density drifts to lower values are considered superfluous and removed, leading to an optimization of the part shape. This manuscript presents a study on how the parameters governing the voxel pruning affect the convergence speed and performance of the attained shape. A stronger penalization factor establishes the criteria by which thin voxels are considered void. In addition, the filter discourages punctured, chessboard pattern regions. The SIMP algorithm produces a forecasted density map on the whole piece voxels. A post-processing is applied to effectively eliminate voxels with low density, to obtain the effective shape. In the literature, mechanical performance finite element analyses are conducted on the full voxel set with diluted densities by linearly weakening each voxel resistance according to its diluted density. Numerical tests show that this approach predicts a more favorable mechanical performance as compared with the one obtained with the shape which actually lacks the voxels with low density. This voxel density - based optimization is particularly convenient for additive manufacturing, as shown with the piece actually produced in this work. Future endeavors include different evolution processes, albeit based on variable density voxel sets, and mechanical tests conducted on the actual sample produced by additive manufacture.*

**CCS Concepts**

•***Applied computing*** → *Computer-aided manufacturing;* •***Computing methodologies*** → *Modeling and simulation;*

## Glossary

| Term | Description | Units |
|---|---|---|
| FEA | Finite element analysis | N/A |
| $\eta \in (0,1)$ | Fraction of mass to be retained in the final design | Adimensional |
| $p \geq 1$ | Penalty factor aimed to polarize element relative densities around 0 and 1 | Adimensional |
| $R \geq 0$ | Filter radius used to discourage chessboard voxel patterns | Adimensional |
| $M_0$ | Initial mass of the domain | g |
| $M$ | Mass function of the domain | g |
| c | Compliance function of the domain | $\mu$J |

† Corresponding author. Paseo Mikeletegi, 57. San Sebastian, Spain. amoreno@vicomtech.org

## 1. Introduction

Shape Optimization usually includes the set up of physical demands (stress, abrasion, vibration, light, heat, temperature, etc.) on the desired object and a domain evolution (reduction, in most publications). Evolution takes place until some constraint domain is satisfied, both in terms of remaining volume and of responses to the demands.

This paper uses the term *shape optimization* as encompassing both *geometry* and *topology* aspects. The reason for this usage is that when voxel densities in one region vanish (geometry change), a side effect may be the creation of holes or disjoint portions, which are topological changes. Therefore, topological changes derive in natural form from geometry changes. Fig. 1 shows an example of the application of shape optimization to a fixed beam subjected to a linear distributed load.

The strategy SIMP (Solid Isotropic Microstructure with Penalization [Sig01, LT14]) implies setting up of a goal percentage of domain volume reduction, the decomposition of the domain in fi-





DOI: 10.2312/ceig.20191201

nite elements, the load and boundary conditions. For the purpose of the present discussion one may assume that the finite elements are voxels. In each iteration of the algorithm, the density of each voxel is re-considered to minimize the compliance of the piece, always keeping the piece mass (i.e. summation of density times voxel volume) below a certain level.

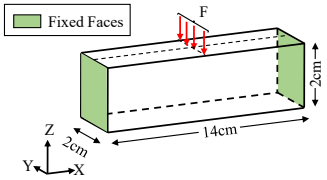


(a) Design domain and boundary conditions.

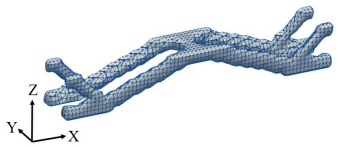


(b) Example of the application of voxel density algorithms for shape optimization.

**Figure 1:** *Design domain and result of the application of shape optimization.*

The voxel density strategy uses a parameter $p$ to polarize the densities of the finite elements towards 0 and 1. It also uses a filter (parameter $R$) which discourages puncturing or chessboard effects that would produce low and high density voxels mixing in a non-dense pattern. The goal is, therefore, to have voxel - density - homogeneous regions.

This paper studies the influence of the parameters of the density-based algorithm, which is one of the most used structural optimization algorithms in additive manufacturing. For this purpose, a case study in the field of solid mechanics is defined. This paper evaluates the impact of the density-based algorithm parameters, not only in the geometry of the final design, but also in the structural performance and computation time.

The rest of the paper is organized as follows: Section 2 provides a review of the related literature. Section 3 describes the methodology used for testing the influence of the studied parameters. Section 4 presents and discusses the obtained results. Finally, Section 5 concludes the work and proposes some potential lines for future research.

## 2. Literature Review

Section 2.1 shows the development of visualization tools to assist manufacturing processes. Subsequently, Section 2.2 presents the use of structural optimization for additive manufacturing. Section 2.3 introduces the studies on the effects of the optimization parameters in the solution given by the voxel density algorithm. Finally, Section 2.4 concludes the literature review and synthesize the contributions of this work.

### 2.1. Structural Optimization and Visual Computing

Structural optimization may be traced back to the work in Ref. [Ben89] and has evolved rapidly since the beginning of the 2000's. Applications in aerospace [SB11], fluid flow [KPEM10] and biomedicine [SPMN10] show the adoption of structural optimization in different fields. The reader is referred to the works in Refs. [DG14, SM13] for a more detailed review. Section 2.2 discusses the use of structural optimization in manufacturing.

In recent years, different tools of visual computing have started to support structural optimization and manufacturing [MHSL18, MMA*14, WWZW16], proving that visual computing is a core technology of Industry 4.0 [PTB*15]. This paper states the mathematical and algorithmic background for the development of an interactive and intuitive tool to assist the process of structural optimization in additive manufacturing.

### 2.2. Structural Optimization for Additive Manufacturing

Although structural and shape optimization impact diverse manufacturing methods, additive manufacturing is particularly convenient for materializing voxel scale optimization. In the context of additive manufacturing, optimization is conducted by (a) growing / clipping the shape (i.e. bi-directional evolutionary structural optimization -BESO [TKZ15, TDZZ18, MZARS*19]), (b) tuning the density of spatial neighborhoods ( [Lan16, PAHA18, ZCX19]), (c) using level sets to determine infill and shell profiles ( [LYT18,FLGX19]), and (d) tuning diameters (proportional topology [CZB*17]).

Voxel density as tuning parameter has been used along level sets as supports for shape optimization in the context of additive manufacturing ( [LM16]). Voxel density variations are relevant in various additive manufacturing aspects, such as: (1) minimization of support structures during the material deposition stages, (2) generation of lattice and porous structures for weight reduction, and (3) tailoring part designs for additive manufacturing.

Ref. [Lan16] presents neighborhood density optimization which hosts elimination of deposition stage support structures. Ref. [PAHA18] maps density maps onto lattice materials suited for shape optimization. Ref. [ZCX19] finds voxel density maps which optimize shape, while at the same time integrates an overhang constraint into the formulation of the shape optimization with additive manufacturing.

### 2.3. Effect of the Parameters in Voxel-density Algorithms

As shown in the previous section, voxel density algorithms have been used in structural optimization for different and varied applications. However, it is not clear how the parameters associated to the optimization process affect, not only the topology and geometry of the final design, but also other relevant variables, such as the convergence speed, objective function, and structural performance of the obtained design.

The impact of the penalization factor $p$ in the geometry of the final design has been widely studied. It is known that large penalization factors ($p > 3$) tend to produce black–and–white de-

signs [Sig01, LT14, DHV09, AAH*10, GWH17, VBSDC18]. However, the influence of the penalization factor on the behavior of other variables (e.g. compliance and von Mises stress) has not been established.

On the other hand, it is common to use filtering techniques to reduce the checkerboard patterns that result from numerical instabilities of the density-based methods [BS04]. In this case, a filtering radius $R$ must be included. This parameter defines the area of the neighborhood in which the filter is applied. The larger the filtering radius $R$, the simpler the geometry of the final shape [GAV16, GWH17]. However, the impact of this parameter on the compliance, time of convergence and structural performance is not well studied yet.

Ref. [GAV16] studies the effects of the variation of the goal volume/mass fraction in the geometrical complexity of the obtained designs. Refs. [EKB07, AAH*10] state that different designs can be obtained by varying the initial density distribution. Besides, other parameters concerning the finite element analysis (FEA) are also studied. Ref. [DHV09] shows the advantage of quadratic finite elements over the linear ones for avoiding checker-board patterns and Ref. [EKB07] exhibits the mesh density dependency of the geometry of the final solution. However, these analyses mainly focus on the geometry of the final shape, leaving aside the structural and mechanical performance of the piece.

### 2.4. Conclusions of the Literature Review

The interest of the additive manufacturing community to advance towards structurally optimal designs has been shown. Different structural optimization algorithms (e.g. density-based, level set, evolutionary structural optimization) have been used in the context of additive manufacturing. However, the success of the optimization is highly dependent on the chosen parameters associated to the algorithm.

This paper focuses on getting a better understanding on how the parameters of the voxel density method affect (1) the behavior of the algorithm and, (2) the geometry and structural performance of the obtained design. This literature review has shown that exist few works that tackle this task. Most of the studies limit to evaluate only changes on the final geometry.

This work assess (1) the speed of convergence of the algorithm, (2) the final compliance, (3) the final maximum von Mises stress and, (4) the geometry and manufacturability of the final shape. As opposed to the found in previous works—in which the tested design is the voxel density map—measurements are also taken on the final piece.

## 3. Methodology

### 3.1. Tuning of Element Density

The objective of the classical structural optimization algorithms is to minimize the amount of material of a design so that it remains functional. In particular, density-based methods for shape optimization are heuristic strategies that aim to find the optimal distribution of the relative densities ($x_i$) of the FEA elements along the domain.

In order to avoid FEA elements with intermediate (gray) densities—i.e. densities that are neither close to 0 nor 1—, voxel density methods adopt the heuristic rule in Eq. 1:

$$E_i = x_i^p E_0 \tag{1}$$

where $p$ is the penalization power for intermediate densities and, $E_i$ and $E_0$ are the elastic moduli of the $i$–th element and the raw material, respectively.

The formulation for the minimization of compliance in Eq. 2 ( [Sig01, LT14]) assumes that the domain is (1) rectangular prismatic, and (2) discretized into $N$ cubic FEA elements (voxels):

$$\begin{aligned} \underset{\mathbf{X}}{\text{minimize}} \quad & \mathrm{c}(\mathbf{X}) = \mathbf{U}^{\mathrm{T}}\mathbf{K}\mathbf{U} \\ \text{subject to} \quad & M(\mathbf{X}) \leq \eta M_0, \\ & \mathbf{K}\mathbf{U} = \mathbf{F}, \\ & 0 < x_{\min} \leq x_i \leq 1, i = 1, \ldots, N. \end{aligned} \tag{2}$$

where $\mathbf{X} = [x_1, \ldots, x_N]^{\mathrm{T}}$ is the vector of relative densities, $x_{\min}$ is the minimum value that the relative density can reach (non-zero to avoid discontinuities that can produce numerical issues), $\mathrm{c}(\mathbf{X})$ is the compliance function, $\mathbf{U}$ is the global displacement vector, $\mathbf{F}$ is the global force vector, $\mathbf{K}$ is the global stiffness matrix, $M_0$ is the mass of the initial design domain, $\eta$ is the fraction of mass that aims to be retained in the final design and $M(\mathbf{X})$ is the mass function (Eq. 3),

$$M(\mathbf{X}) = \frac{M_0}{N} \sum_{i=1}^{N} x_i. \tag{3}$$

Most of the implementations of the voxel density algorithms also include filtering techniques to avoid checkerboard patterns and, mesh-dependent solutions [Sig01]. One of the most frequently used filters is the *sensitivity filter*, which operates on the derivatives of the compliance function, as shown in Eq. 4 [Sig01]:

$$\widetilde{\frac{\partial \mathrm{c}}{\partial x_i}} = \frac{\sum_{j \in N_i} H_{ij} \frac{\partial \mathrm{c}}{\partial x_j} x_j}{x_j \sum_{j \in N_i} H_{ij}}, \tag{4}$$

where $N_i = \{j : \mathrm{dist}(i, j) \leq R\}$ is the neighborhood of the $i$-th element and $R$ is the filter radius and, $H_{ij}$ is a weight factor defined in Eq. 5:

$$H_{ij} = R - \mathrm{dist}(i, j), \tag{5}$$

where $\mathrm{dist}(i, j)$ is the distance between the centers of the elements $i$ and $j$ ($c_i$ and $c_j$, respectively), divided by the length $l$ of the FEA elements (Eq. 6):

$$\mathrm{dist}(i, j) = \frac{||c_i - c_j||}{l}. \tag{6}$$

### 3.2. Conversion of the Voxel Density Map to the Design-for-Manufacturing

The output of the implemented heuristic algorithm is a density map (Fig. 2(a)) in which each voxel $i$ has an associated relative density $x_i$ ($0 \leq x_i \leq 1$). In general, this design cannot be manufactured. In order to select the elements to manufacture, this paper employes the algorithm presented in Ref. [SM13]. The algorithm finds the minimum density threshold $x_T$ that guarantees the mass constraint

for the design-for-manufacturing (also called black-and-white design). The surviving elements are those for which $x_i \geq x_T$. Fig. 2 shows an example of the conversion of the voxeld density map to the design-to-manufacturing.

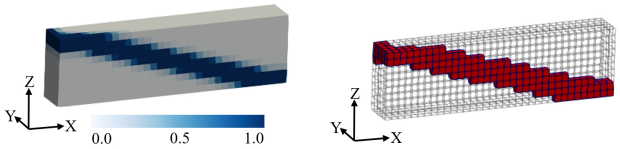


(a) Voxel density map. (b) Black-and-white domain.

**Figure 2:** *Conversion of the voxel density map to the design-to-manufacture.*

### 3.3. Sensitivity Analysis

The formula in Eq. 7 allows the numerical analysis of the sensitivity of the function $F$ with respect to the parameter $\alpha$:

$$S_\alpha^F = \frac{\partial \ln F}{\partial \ln \alpha} = \frac{\alpha}{F}\frac{\partial F}{\partial \alpha} \approx \frac{\overline{\alpha}}{\overline{F}}\frac{\Delta F}{\Delta \alpha}, \tag{7}$$

where $\Delta\alpha$ and $\Delta F$ denote small changes in the value of $\alpha$ and $F$; and $\overline{\alpha} = \alpha + \Delta\alpha/2$, $\overline{F} = (F_\alpha + F_{\alpha+\Delta\alpha})/2$.

In this paper, the functions $F$ to analyze are: compliance, maximum von Mises stress and number of iterations. Likewise, the parameters $\alpha$ to study are $p$ and $R$.

Relative sensitivity allows to study how slight variations in the value of the parameters can affect the mechanical performance of the final piece.

Von Mises stress is used in solid mechanics as a failure criterion and it is desirable to minimize it. Von Mises stress is defined as per Eq. 8:

$$\sigma_{VM} = \sqrt{\frac{(\sigma_1 - \sigma_2)^2 + (\sigma_2 - \sigma_3)^2 + (\sigma_3 - \sigma_1)^2}{2}}, \tag{8}$$

where $\sigma_1, \sigma_2$ and $\sigma_3$ are the principal stresses.

### 3.4. Case Study

This paper uses a case study for the analysis of the effects of the algorithm parameters. This section describes: (1) the domain and material used for the simulations and, (2) the configuration of the numerical tests.

#### 3.4.1. Domain of Analysis and Material Characterization

The studied domain is a 3D fixed beam with linearly distributed load applied in the center of the top face (see Fig. 1(a)). The beam has size 140.0mm x 20.0mm x 20.0mm and the magnitude of the total applied load is 1.1N. The material employed for the simulations is a PLA filament of a commercial brand. The properties of this material are presented in Table 1.

**Table 1:** *Properties of the PLA filament used for the simulations.*

| Property | Value |
|---|---|
| Young's modulus | 1230 MPa [BQ18] |
| Poisson's ratio | 0.33 [FAL16] |
| Density | 1.24 g/cm$^3$ [BQ18] |

The domain in Fig. 1(a) is symmetric to the planes depicted in Figs. 3(a) and 3(b). Therefore, it can be simplified to the domain in Fig. 3(c). The equivalent load case is shown in Fig. 4.

In order to show the equivalence of the load cases presented in Figs. 1(a) and 4, a FEA simulation is executed for each domain, using $F = 1.1$N. Results of the simulations are presented in Fig. 5. Notice how the displacements of the two load cases are equivalent. This result allows to execute the simulations of the shape optimization algorithm on the simplified domain.

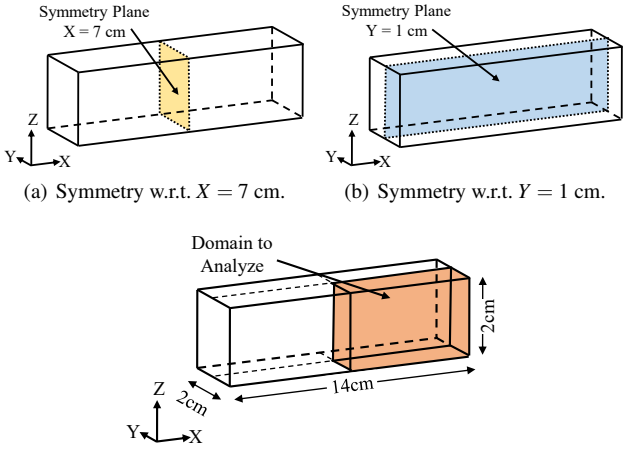


(a) Symmetry w.r.t. $X = 7$ cm. (b) Symmetry w.r.t. $Y = 1$ cm.

(c) Simplified domain.

**Figure 3:** *Simplification of the domain in Fig. 1(a).*

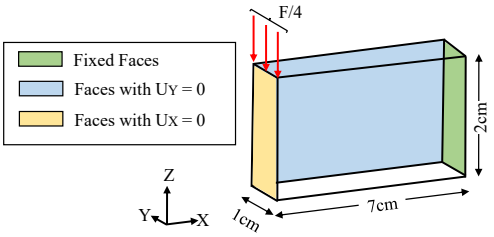


**Figure 4:** *Design domain and boundary conditions. Simplified domain.*

### 3.5. Set-up of Numerical Experiments

This paper conducts studies of the effects of $p$ (density polarization) and $R$ (region homogenization) parameters upon the piece geometry and mechanical performance, in the scenario of voxel density optimization methods. Table 2 presents the set of different sim-

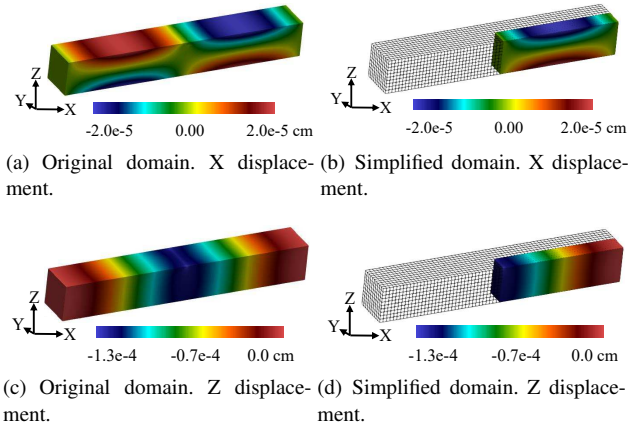


(a) Original domain. X displacement. (b) Simplified domain. X displacement. (c) Original domain. Z displacement. (d) Simplified domain. Z displacement.

**Figure 5:** *Comparison of the X and Z displacements for the original and simplified domain.*

ulations used for the study of each parameter. The measured variables for each simulation are: (1) compliance, (2) maximum von Mises stress and, (3) convergence speed, measured by the number of iterations. The authors implemented the heuristic voxel density optimization method in C++. The implementation uses the optimality criteria for updating the variables within the optimizer [Ben95].

To execute the FEA simulations, the domain in Fig. 4 is discretized into 1750 voxels (35x5x10). Subsequently, the FEA mesh is obtained by converting every voxel into a regular hexahedral (cubic) FEA element.

## 4. Results and Discussion

Sections 4.1 and 4.2 discuss the influence of the penalty factor $p$ and the filter radius $R$ in the manufacturability, compliance and maximum von Mises stress of the final design, so as the convergence speed of the algorithm. Measurements are executed on both the voxel density map and the black-and-white design. Subsequently, Section 4.3 presents a sensitivity analysis of the studied variables with respect to $p$ and $R$. Finally, Section 4.4 shows some of the specimens generated using different parameter configurations.

### 4.1. Influence of the Penalty Factor in the Geometry, Manufacturability and Mechanical Performance of the Design

To evaluate the influence of the penalty factor $p$ in the geometry and structural performance of the final design, 14 simulations were executed varying the value of $p$ between 1.0 and 7.5, as shown in Table 2. Figs. 6(a), 6(b) and 6(c) show the resultant density field for $p = 1.0$ (no penalty), $p = 3.0$ and, $p = 7.0$. Histograms in Figs. 6(d), 6(e) and 6(f) depict the frequency distribution of the density values. Notice that for $p = 1.0$, density distribution is concentrated in the interval $(0.0, 0.2)$. On the other hand, for $p = 3.0$ and $p = 7.0$, the largest bars are for $x_i = 0.0$ and $x_i = 1.0$. These density distributions show the action of the penalty factor to eliminate the intermediate densities.

**Table 2:** *Values of the parameters used for the numerical simulations.*

| Analyzed parameter | Parameter value | | | |
|---|---|---|---|---|
| | $p$ | $R$ | $\eta$ | $M_0$ |
| $p$ | $\{1.0, 1.5, \ldots, 7.5\}$ | 1.0 | 0.1 | 17.4 g |
| $R$ | 3.0 | $\{0, 1, \ldots, 5\}$ | 0.1 | 17.4 g |

Figs. 6(g), 6(h) and 6(i) display the black-and-white design for $p = 1.0$, $p = 3.0$ and, $p = 7.0$. The design for $p = 1.0$ is composed by multiple non-connected parts and cannot be manufactured. The differences in the designs for $p = 3.0$ and $p = 7.0$ show that larger values of $p$ tend to produce simpler geometries.

Fig. 7(a) shows the compliance of the gray and black-and-white designs of the 14 simulations varying $p$. For $p = 1.0$ and $p = 1.5$, the black-and-white domains are not connected and, therefore, compliance is not reported. Notice that for the gray domain, compliance tends to increase as $p$ increases. However, for the black-and-white design, compliance converges to a value close to 4.0 $\mu$J.

Fig. 7(b) displays the maximum von Mises stress for the gray and black-and-white domains. So as in the case of compliance, maximum von Mises stress has a different behavior for the gray and black-and-white designs. In the case of the gray domain, maximum von Mises stress tends to increase, even for $p \geq 2.0$. On the other hand, for the black-and-white domain, maximum von Mises stress oscillates around 100 kPa.

For the studied gray domains, the compliance and maximum von Mises stress attain their lowest values when $p = 1.0$ and $p = 1.5$. However, for these values of $p$, the respective black-and-white domains cannot be manufacture. It exhibits that the results for the black-and-white domain are not necessarily in concordance with the results for the gray domain. It demonstrates the importance of analyzing the black-and-white domain, which is the one to be manufactured.

In Fig. 7(c) can be seen the number of iterations that the algorithm needed to converge for every value of $p$. The reader can see that, for the domains that can be manufactured ($p > 2.5$), large values of $p$ tend to accelerate the convergence of the algorithm.

### 4.2. Influence of the Filter Radius in the Geometry, Manufacturability and Mechanical Performance of the Design

To study the influence of the filter radius $R$, it was varied between 0.0 and 6.0. Figs. 8(a), 8(b) and 8(c) show the resultant density field for $R = 0.0$ (no filtering), $R = 1.0$ and, $R = 3.0$. Figs. 8(d), 8(e) and 8(f) show the corresponding histograms of the density maps: when $R$ increases, the density is distributed more evenly along the domain and, therefore, more intermediate densities appear.

The black-and-white domains for $R = 0.0$, $R = 1.0$ and, $R = 3.0$ are displayed in Figs. 8(g), 8(h) and 8(i). Complex and detailed geometries are attained for small values of $R$. However, the geometrical complexity stimulates the appearance of non-manufacturable sub-domains. Fig. 12(c) show that for $R = 0.0$ appear voxels that

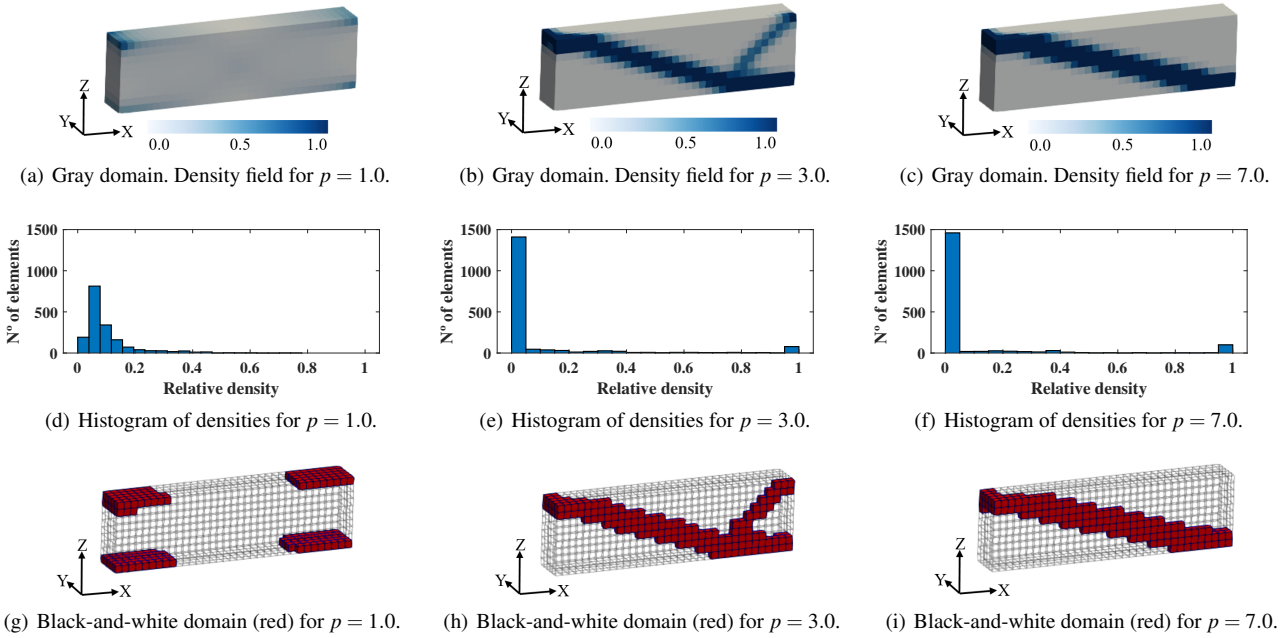


(a) Gray domain. Density field for $p = 1.0$. (b) Gray domain. Density field for $p = 3.0$. (c) Gray domain. Density field for $p = 7.0$.

(d) Histogram of densities for $p = 1.0$. (e) Histogram of densities for $p = 3.0$. (f) Histogram of densities for $p = 7.0$.

(g) Black-and-white domain (red) for $p = 1.0$. (h) Black-and-white domain (red) for $p = 3.0$. (i) Black-and-white domain (red) for $p = 7.0$.

**Figure 6:** *Impact of the penalty factor in the geometry and manufacturability.*

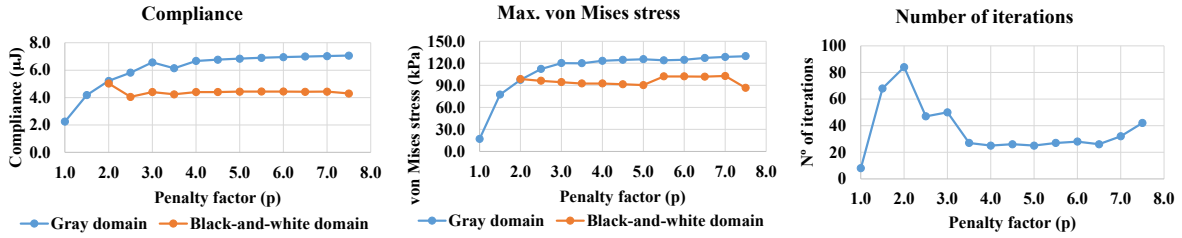


(a) Compliance. (b) Maximum von Mises stress. (c) Convergence speed.

**Figure 7:** *Impact of the penalty factor in the convergence speed and mechanical performance.*

are connected by a single edge, which impedes the correct manufacturing (even using additive manufacturing technologies) of the piece. The occurrence of these chessboard patterns are associated to numerical errors that may be caused by the voxel discretization and the type of FEA element used for the simulations [PQR05].

The compliance and maximum von Mises stress are shown in Figs. 9(a) and 9(b). For $R = 5.0$, compliance and maximum von Mises stress are not reported for the black-and-white domain because the domain is not connected. The increase of the compliance for the gray domain (Fig. 9(a)) for increments in $R$ is noticeable. However, the value of $R$ does not affect the compliance of the black-and-white domain.

So as in the previous section, the behavior of the compliance and maximum von Mises stress is different for the black-and-white and gray domains. The mechanical performance of the gray domain is merely illustrative and does not represent a real piece. Therefore, it is necessary to check the performance of the piece for manufacturing. This finding shows the relevance of a stage of validation in the pipeline of structural optimization.

Fig. 9(b) shows that larger values of $R$ produce structures with larger maximum von Mises stress for the black-and-white domain. This result agrees with the result for the gray domain when $R \leq 3.0$. However, for $R \geq 4.0$, the maximum von Mises stress of the gray domain decays. It is related to the more even distribution of the relative densities in the volume.

Fig. 9(c) shows the convergence speed of the algorithm depending on the value of $R$. No filtering and large filter radii contribute to a faster convergence. However, the final design may not be manufacturable. Therefore, intermediate values of $R$ should be selected.

### 4.3. Sensitivity Analysis

Fig. 10 presents the relative sensitivity of the compliance, maximum von Mises stress and number of iterations with respect to the

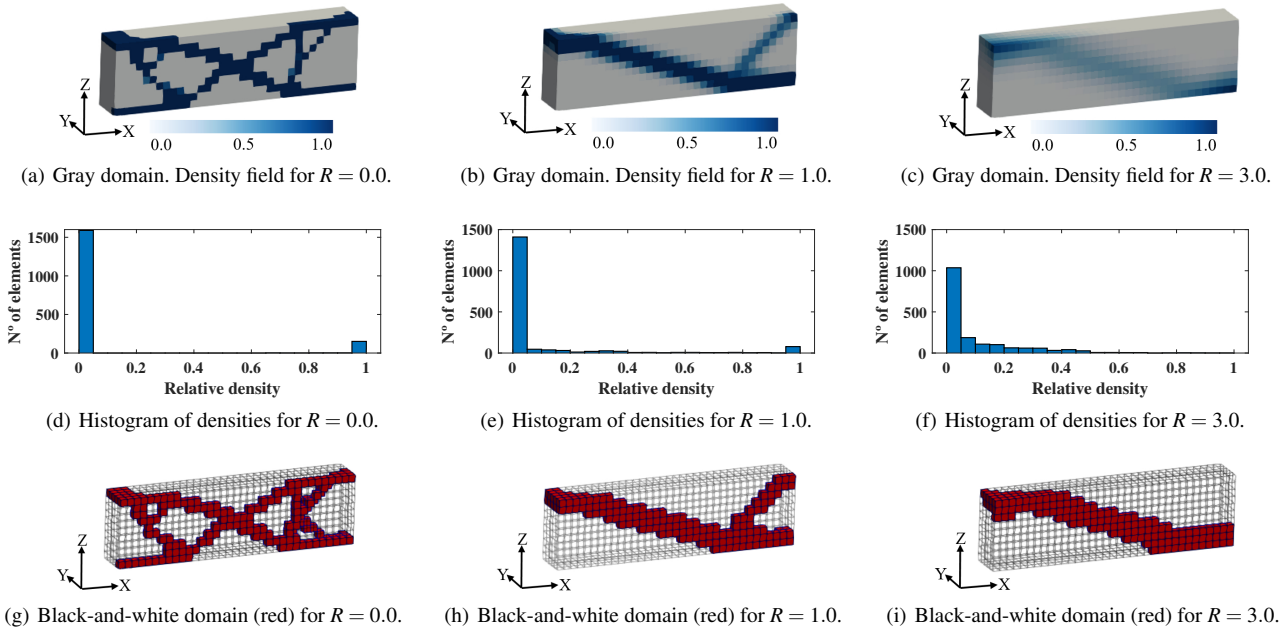


(a) Gray domain. Density field for $R = 0.0$. (b) Gray domain. Density field for $R = 1.0$. (c) Gray domain. Density field for $R = 3.0$.

(d) Histogram of densities for $R = 0.0$. (e) Histogram of densities for $R = 1.0$. (f) Histogram of densities for $R = 3.0$.

(g) Black-and-white domain (red) for $R = 0.0$. (h) Black-and-white domain (red) for $R = 1.0$. (i) Black-and-white domain (red) for $R = 3.0$.

**Figure 8:** *Impact of the radius filter in the geometry and manufacturability.*

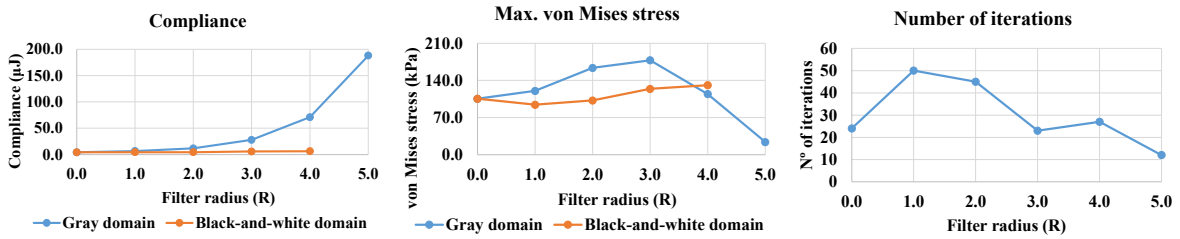


(a) Compliance. (b) Maximum von Mises stress. (c) Convergence speed.

**Figure 9:** *Impact of the filter radius in the convergence speed and mechanical performance.*

parameter $p$. To calculate these values, $R$ was fixed to 1.0. It is noticeable that for $p > 4.0$, the compliance and the maximum von Mises stress are not affected by the value of $p$. On the other hand, the convergence speed of the algorithm is very sensitive to the value of $p$.

Fig. 11 displays the sensitivity analysis of the parameter $R$ for the studied variables: compliance, maximum von Mises stress and convergence speed. From Figs. 11(a) and 11(b) can be infered that $R$ does not have much influence on the compliance and maximum von Mises stress of the final design. However, $R$ does impact the mechanical performance of the voxel density map, specially for larger values of $R$. Convergence speed is also affected when $R \geq 2.0$.

### 4.4. Evaluation of the Manufacturability and 3D Printed Pieces

Additive manufacturing allows the production of complicated geometries that cannot be manufactured using other technologies. To evaluate the feasibility of the designs produced by the voxel density algorithm, three resultant domains of Sections 4.1 and 4.2 were selected. Figs. 12(a)–12(c) show the corresponding STL model of each design. The domain in Fig. 12(c) has neighborhoods in which the voxels are connected only by an edge, which compromises the manufacturability of the piece.

Figs. 12(d)–12(f) show the 3D printed pieces obtained from the STL models in Figs. 12(a)–12(c). Notice that for the first two domains, the geometry of the shape can be reproduced accurately. However, due to the single edge's connections in the third design, some sub-domains disconnect when support material is removed. In order to improve the manufacturability of the final piece, different solutions for suppressing these punctured or chessboard-looking regions have been proposed. Filtering techniques (as the implemented in this work), the use of higher–order FEA elements and the deletion of single-edge or single vertex connections [PQR05] are some of the plausible solutions. Other possible solution is to smooth the voxel design. This work uses the March-

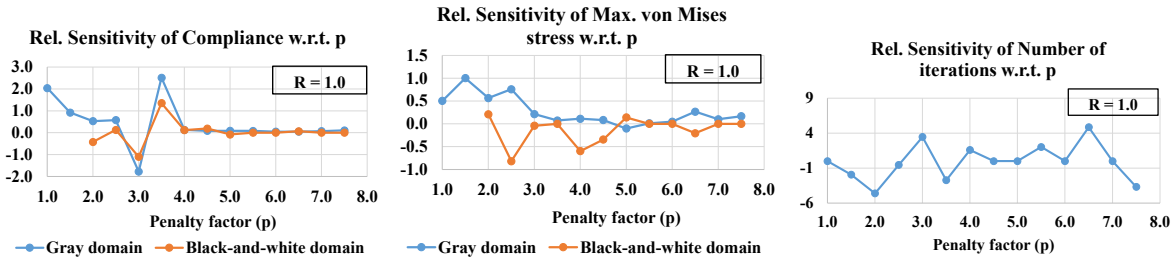


(a) Sensitivity of compliance. (b) Sensitivity of maximum von Mises stress. (c) Sensitivity of the number of iterations.

**Figure 10:** *Relative sensitivity of the compliance, maximum von Mises stress and convergence speed w.r.t. p.*

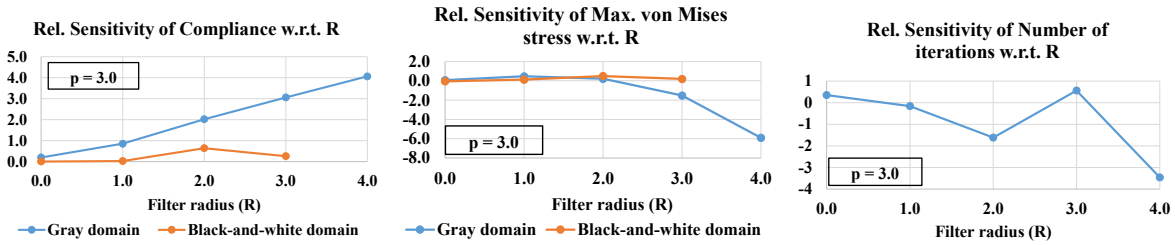


(a) Sensitivity of compliance. (b) Sensitivity of maximum von Mises stress. (c) Sensitivity of the number of iterations.

**Figure 11:** *Relative sensitivity of the compliance, maximum von Mises stress and convergence speed w.r.t. R.*

ing Cubes algorithm to smooth the surface associated to the voxel domain. Figs.13 show the obtained STL models after smoothing the domains in Fig. 12 and the corresponding 3D-printed pieces.

## 5. Conclusions

This paper presents analysis of the effects of the parameters of the heuristic voxel density algorithms in (1) the geometry and structural performance of the final design and, (2) the convergence speed of the algorithm. For the study, the authors use one set-up, therefore conclusions on the detailed behavior of the parameters may not be drawn. However, results show that (a) extreme values of the parameters may affect the manufacturability and mechanical performance of the designs and (b) mechanical analyses must be executed on the domain-to-manufacture and not in the *optimal* voxel density map given by the algorithm.

Shape optimization is an intermediate step in the work-flow of the design-to-manufacturing. In this realm, it is important to understand how the shape optimization algorithms work and how their parameters affect the obtained design. This work can be a worthy tool for many designers and engineers that use commercial software that implements density-based methods.

### 5.1. Limitations

This work studies the effects of the penalty power $p$ and the filter radius $R$ independently. It may be interesting to understand the interaction between these two parameters. Future research should address the analysis of simultaneous changes in the values of $p$ and $R$. Moreover, other parameters (e.g. mass fraction $\eta$) can be investigated. Physical experimentation is also required for testing the correctness and exactitude of the numerical results.

### 5.2. Future Work

The authors look forward to generate an interactive tool to assist the design process in additive manufacturing. The tool would allow designers to visualize different different pieces and their mechanical performance. It has to be capable of generating different configurations for the domain, loads, constraints and parameter configurations for shape optimization.

It is necessary to validate the conclusions drawn in this work. In that sense, there are three lines of research that are open for further work: (1) the simulation of other domains with different load cases, (2) the analysis of interactions between $p$ and $R$ and (3) physical tests to confirm numerical results.

## References

[AAH*10] AREMU A., ASHCROFT I., HAGUE R., WILDMAN R., TUCK C.: Suitability of SIMP and BESO topology optimization algorithms for additive manufacture. In *21st Annual International Solid Freeform Fabrication Symposium (SFF)–An Additive Manufacturing Conference* (2010), pp. 679–692. 3

[Ben89] BENDSØE M. P.: Optimal shape design as a material distribution problem. *Structural optimization 1*, 4 (Dec 1989), 193–202. doi:10.1007/BF01650949. 2

[Ben95] BENDSØE M. P.: *The homogenization approach to topology design*. Springer Berlin Heidelberg, Berlin, Heidelberg, 1995, pp. 5–77. doi:10.1007/978-3-662-03115-5_2. 5

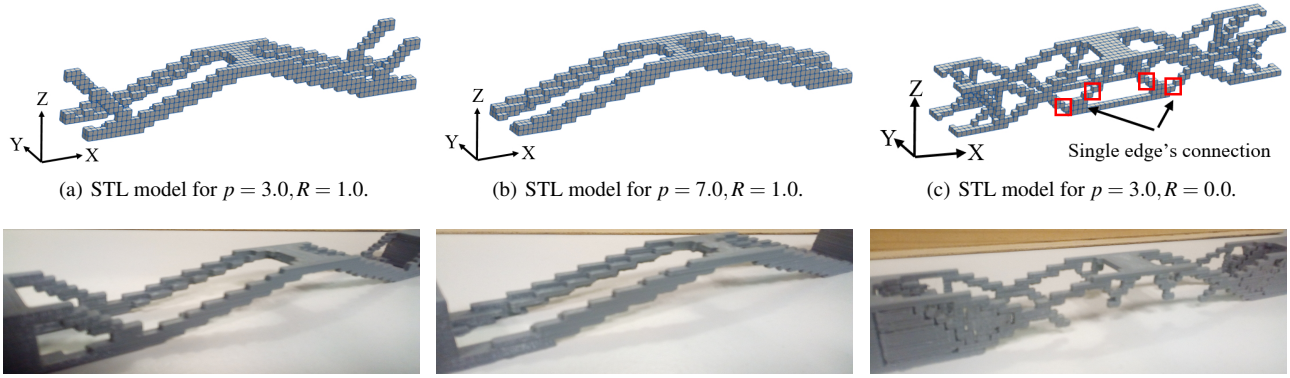


(a) STL model for $p = 3.0, R = 1.0$. (b) STL model for $p = 7.0, R = 1.0$. (c) STL model for $p = 3.0, R = 0.0$.

(d) Printed version of model in Fig. 12(a). (e) Printed version of model in Fig. 12(b). (f) Printed version of model in Fig. 12(c).

**Figure 12:** *3D printed designs obtained using the voxel density algorithm.*

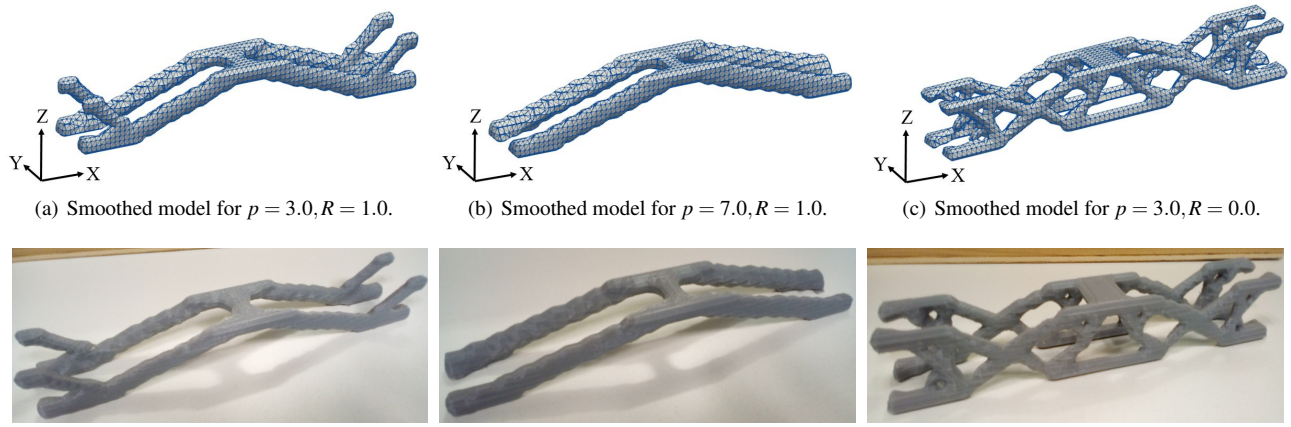


(a) Smoothed model for $p = 3.0, R = 1.0$. (b) Smoothed model for $p = 7.0, R = 1.0$. (c) Smoothed model for $p = 3.0, R = 0.0$.

(d) Printed version of model in Fig. 13(a). (e) Printed version of model in Fig. 13(b). (f) Printed version of model in Fig. 13(c).

**Figure 13:** *Smoothed designs using Marching Cubes algorithm and the corresponding 3D printed pieces.*

[BQ18] BQ: PLA filament: technical datasheet, 2018. https://www.bq.com/en/support/pla-premium/support-sheet. URL: https://www.bq.com/en/support/pla-premium/support-sheet. 4

[BS04] BENDSØE M. P., SIGMUND O.: *Topology optimization by distribution of isotropic material*. Springer Berlin Heidelberg, Berlin, Heidelberg, 2004, pp. 1–69. doi:10.1007/978-3-662-05086-6_1. 3

[CZB*17] CHENG L., ZHANG P., BIYIKLI E., BAI J., ROBBINS J., TO A.: Efficient design optimization of variable-density cellular structures for additive manufacturing: theory and experimental validation. *Rapid Prototyping Journal 23*, 4 (2017), 660–677. doi:10.1108/RPJ-04-2016-0069. 2

[DG14] DEATON J. D., GRANDHI R. V.: A survey of structural and multidisciplinary continuum topology optimization: post 2000. *Structural and Multidisciplinary Optimization 49*, 1 (Jan 2014), 1–38. doi:10.1007/s00158-013-0956-z. 2

[DHV09] DADALAU A., HAFLA A., VERL A.: A new adaptive penalization scheme for topology optimization. *Production Engineering 3*, 4 (2009), 427. doi:10.1007/s11740-009-0187-8. 3

[EKB07] EDWARDS C. S., KIM H. A., BUDD C. J.: An evaluative study on ESO and SIMP for optimising a cantilever tie—beam. *Structural and Multidisciplinary Optimization 34*, 5 (2007), 403–414. doi:10.1007/s00158-007-0102-x. 3

[FAL16] FARAH S., ANDERSON D. G., LANGER R.: Physical and mechanical properties of PLA, and their functions in widespread applications–a comprehensive review. *Advanced Drug Delivery Reviews 107* (2016), 367 – 392. doi:10.1016/j.addr.2016.06.012. 4

[FLGX19] FU J., LI H., GAO L., XIAO M.: Design of shell-infill structures by a multiscale level set topology optimization method. *Computers & Structures 212* (2019), 162 – 172. doi:10.1016/j.compstruc.2018.10.006. 2

[GAV16] GARAIGORDOBIL A., ANSOLA R., VEGUERÍA E.: Study of topology optimization parameters and scaffold structures in additive manufacturing. In *Proceedings of the VII European Congress on Computational Methods in Applied Sciences and Engineering* (2016), National Technical University of Athens, pp. 3700–3710. doi:10.7712/100016.2066.6404. 3

[GWH17] GEBREMEDHEN H. S., WOLDEMICHAEL D. E., HASHIM F. M.: Effect of modeling parameters in SIMP based stress constrained structural topology optimization. *International Journal of Mechanical and Mechatronics Engineering 17*, 6 (2017), 32–39. 3

[KPEM10] KREISSL S., PINGEN G., EVGRAFOV A., MAUTE K.: Topology optimization of flexible micro-fluidic devices. *Structural*

*and Multidisciplinary Optimization 42*, 4 (Oct 2010), 495–516. doi:10.1007/s00158-010-0526-6. 2

[Lan16] LANGELAAR M.: Topology optimization of 3D self-supporting structures for additive manufacturing. *Additive Manufacturing 12* (2016), 60 – 70. doi:10.1016/j.addma.2016.06.010. 2

[LM16] LIU J., MA Y.: A survey of manufacturing oriented topology optimization methods. *Advances in Engineering Software 100* (2016), 161 – 175. doi:10.1016/j.advengsoft.2016.07.017. 2

[LT14] LIU K., TOVAR A.: An efficient 3D topology optimization code written in Matlab. *Structural and Multidisciplinary Optimization 50*, 6 (2014), 1175–1196. doi:10.1007/s00158-014-1107-x. 1, 3

[LYT18] LIU J., YU H., TO A. C.: Porous structure design through Blinn transformation-based level set method. *Structural and Multidisciplinary Optimization 57*, 2 (2018), 849–864. doi:10.1007/s00158-017-1786-1. 2

[MHSL18] MARTÍNEZ J., HORNUS S., SONG H., LEFEBVRE S.: Polyhedral voronoi diagrams for additive manufacturing. *ACM Trans. Graph. 37*, 4 (2018), 129:1–129:15. doi:10.1145/3197517.3201343. 2

[MMA*14] MEJIA D., MORENO A., ARBELAIZ A., POSADA J., RUIZ-SALGUERO O.: Accelerated thermal simulation for three-dimensional interactive optimization of computer numeric control sheet metal laser cutting. *Journal of Manufacturing Science and Engineering 140*, 3 (2014), 031006–031006–9. doi:10.1115/1.4038207. 2

[MZARS*19] MONTOYA-ZAPATA D., ACOSTA D. A., RUIZ-SALGUERO O., POSADA J., SANCHEZ-LONDONO D.: A general meta-graph strategy for shape evolution under mechanical stress. *Cybernetics and Systems 50*, 1 (2019), 3–24. doi:10.1080/01969722.2018.1558011. 2

[PAHA18] PANESAR A., ABDI M., HICKMAN D., ASHCROFT I.: Strategies for functionally graded lattice structures derived using topology optimisation for Additive Manufacturing. *Additive Manufacturing 19* (2018), 81 – 94. doi:10.1016/j.addma.2017.11.008. 2

[PQR05] POMEZANSKI V., QUERIN O., ROZVANY G.: CO–SIMP: extended SIMP algorithm with direct COrner COntact COntrol. *Structural and Multidisciplinary Optimization 30*, 2 (Aug 2005), 164–168. doi:10.1007/s00158-005-0514-4. 6, 7

[PTB*15] POSADA J., TORO C., BARANDIARAN I., OYARZUN D., STRICKER D., DE AMICIS R., PINTO E. B., EISERT P., DÖLLNER J., VALLARINO I.: Visual computing as a key enabling technology for Industrie 4.0 and industrial internet. *IEEE Computer Graphics and Applications 35*, 2 (2015), 26–40. doi:10.1109/MCG.2015.45. 2

[SB11] STANFORD B., BERAN P.: Conceptual design of compliant mechanisms for flapping wings with topology optimization. *AIAA Journal 49*, 4 (2011), 855–867. doi:10.2514/1.J050940. 2

[Sig01] SIGMUND O.: A 99 line topology optimization code written in Matlab. *Structural and Multidisciplinary Optimization 21*, 2 (2001), 120–127. doi:10.1007/s001580050176. 1, 3

[SM13] SIGMUND O., MAUTE K.: Topology optimization approaches. *Structural and Multidisciplinary Optimization 48*, 6 (2013), 1031–1055. doi:10.1007/s00158-013-0978-6. 2, 3

[SPMN10] SUTRADHAR A., PAULINO G. H., MILLER M. J., NGUYEN T. H.: Topological optimization for designing patient-specific large craniofacial segmental bone replacements. *Proceedings of the National Academy of Sciences 107*, 30 (2010), 13222–13227. doi:10.1073/pnas.1001208107. 2

[TDZZ18] TANG Y., DONG G., ZHOU Q., ZHAO Y. F.: Lattice structure design and optimization with additive manufacturing constraints. *IEEE Transactions on Automation Science and Engineering 15*, 4 (2018), 1546–1562. doi:10.1109/TASE.2017.2685643. 2

[TKZ15] TANG Y., KURTZ A., ZHAO Y. F.: Bidirectional Evolutionary Structural Optimization (BESO) based design method for lattice structure to be fabricated by additive manufacturing. *Computer-Aided Design 69* (2015), 91 – 101. doi:10.1016/j.cad.2015.06.001. 2

[VBSDC18] VANTYGHEM G., BOEL V., STEEMAN M., DE CORTE W.: Multi-material topology optimization involving simultaneous structural and thermal analyses. *Structural and Multidisciplinary Optimization* (2018). doi:10.1007/s00158-018-2095-z. 3

[WWZW16] WU J., WANG C. C., ZHANG X., WESTERMANN R.: Self-supporting rhombic infill structures for additive manufacturing. *Computer-Aided Design 80* (2016), 32 – 42. doi:10.1016/j.cad.2016.07.006. 2

[ZCX19] ZHANG K., CHENG G., XU L.: Topology optimization considering overhang constraint in additive manufacturing. *Computers & Structures 212* (2019), 86 – 100. doi:10.1016/j.compstruc.2018.10.011. 2